

Origin of 18-fold quasicrystal

S Bekku¹, P Ziherl^{2,3} and T Dotera¹

¹Department of Physics, Kinki University, 3-4-1 Kowakae Higashi-Osaka 577-8502, Japan

²Faculty of Mathematics and Physics, University of Ljubljana, Jadranska 19, SI-1000 Ljubljana, Slovenia

³Jožef Stefan Institute, Jamova 39, SI-1000 Ljubljana, Slovenia

E-mail: dotera@phys.kindai.ac.jp

Abstract. We investigate the origin of the 18-fold symmetry in quasicrystals. We perform Monte Carlo simulations of 2D disks interacting with the hard-core/square-shoulder potential, and we analyze the bond-orientational order and the local vertex configurations. We find that the so-called special clusters of particles play a crucial role in the mixing of the three sets of bond directions 20° apart, producing the 18-fold diffraction pattern.

1. Introduction

Since soft quasicrystals were discovered in nature [1, 2, 3, 4], a new research front has emerged in the field of quasicrystals. In particular, Fischer *et al.* found that colloidal micelles in solution self-assembled into a 18-fold quasicrystalline phase [5], whose symmetry has not been found in synthetic metallic compounds [6, 7]. They used PI₃₀-PEO₁₂₀ block copolymers based on the hydrophobic polyisoprene (PI) and the hydrophilic polyethylene oxide (PEO). These block copolymers self-assembled into spherical core-shell micelles where the well-defined core of PI blocks is surrounded by a thick shell of PEO blocks. Presently, the real-space structure of quasicrystals formed by these micelles is still not unequivocally determined.

To investigate soft quasicrystals theoretically, we have numerically explored a 2D system of disks with a purely repulsive hard-core/square-shoulder (HCSS) pair interaction [8, 9, 10, 11]

$$V(r) = \begin{cases} \infty, & r < \sigma \\ \varepsilon, & \sigma < r < \lambda\sigma \\ 0, & r > \lambda\sigma \end{cases} . \quad (1)$$

Here ε is the shoulder height and $\lambda\sigma$ and σ are the shoulder and the hard-core diameters, respectively. This two-lengthscale potential is known to stabilize several types of quasicrystals [12, 13, 14, 15, 16, 17], and its shape is described solely by the shoulder-to-core ratio λ .

At a shoulder-to-core ratio of $\lambda \approx 1.27$, we found a high-density phase of 18-fold symmetry [13, 18]. With a large fraction of particles forming close-packed equilateral triangles, the phase is structurally similar to the dodecagonal quasicrystalline phase except that the four-sided tiles that it contains are rhombi rather than squares. The rhombi, whose acute and obtuse angles are 80° and 100°, respectively, consist of two identical isosceles triangles such their bases are equal to $\lambda\sigma$ and their legs are σ . In this paper, we study the structure of the 18-fold phase

in more detail, focusing on the mechanisms of its formation by examining the development of the bond-orientational order parameters at low temperatures.

2. Specific heat and bond-orientational order

We use Monte Carlo (MC) simulations of the NVT ensemble of $N = 4000$ particles in a square box with periodic boundary conditions. We choose the shoulder-to-core ratio of $\lambda = 1.27$ and a packing fraction of $\eta = \pi N \sigma^2 / 4A$, where N is the number of disks in a box of area A . In all results presented here except figure 10, $\eta = 0.77$. The value of $\lambda = 1.27$ was chosen such that the apex angle of the isosceles triangle mentioned above and given by $2 \arcsin(\lambda/2)$ is close to 80° , thereby promoting the 80° - 100° rhombi characteristic of the 18-fold quasicrystal. Inverse temperature is defined by $\beta = \epsilon/k_B T$. The system was equilibrated for 10^7 MC steps at all β between 0 and 5 except for $2.5 < \beta < 4.0$ where 5×10^7 MC steps were performed.

Figure 1 shows the specific heat per particle. The most striking feature of this plot is the sharp peak at $\beta = 3.1$, which indicates a transition. To understand the meaning of this peak, we evaluate the bond-orientational order parameters χ_m defined by

$$\chi_m = \left\langle \left| \frac{1}{N_B} \sum_{\mathbf{r}} \exp(im\theta_{\mathbf{r}}) \right|^2 \right\rangle,$$

where $\theta_{\mathbf{r}}$ is the angle between a reference in-plane direction and the bond connecting particles separated by no more than $\lambda\sigma$ and located at \mathbf{r} ; N_B is the number of nearest-neighbor bonds and angle brackets indicate ensemble average. Based on χ_6 , χ_{12} , and χ_{18} shown in figure 2, one may distinguish between three distinct regimes. For $\beta < 3.1$, all three order parameters decrease with β and χ_6 is considerably larger than χ_{12} and χ_{18} , which indicates a 6-fold phase. The abrupt increase of χ_{18} at $\beta = 3.1$ consistent with the specific-heat peak signals the onset of the intermediate-temperature regime. The subsequent growth of χ_{18} and the continuing decrease of χ_6 and χ_{12} imply a coexistence of 18-fold and 6-fold phase for β between 3.1 and 3.9. The third, low-temperature regime begins at $\beta = 3.9$ where χ_{18} increases again and grows further as β is increased while χ_6 and χ_{12} are 0. This state corresponds to the pure 18-fold phase.

Figure 3 shows the diffraction patterns obtained by computing the Fourier transforms of particles' centers of mass at $\beta = 3.0, 3.2$, and 4.0 , (panels *a*, *b*, and *c*, respectively). These

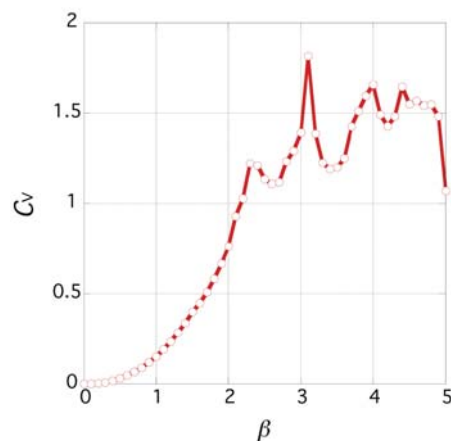


Figure 1. Specific heat C_V per particle *vs.* inverse temperature β ; note the sharp peak at $\beta = 3.1$.

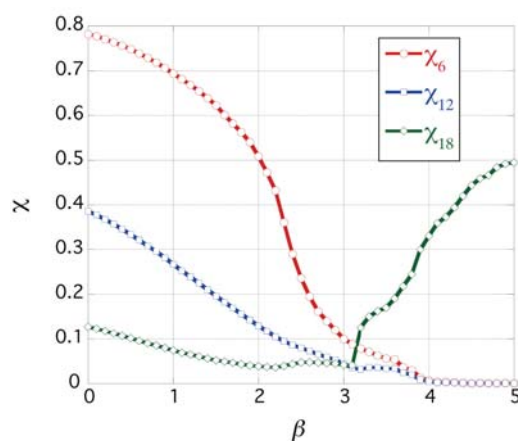


Figure 2. Bond orientational order parameters χ_6 , χ_{12} , and χ_{18} *vs.* β . Beyond $\beta \cong 3.1$, χ_{18} increases whereas χ_6 and χ_{12} are both 0 for $\beta \geq 3.9$.

patterns additionally emphasize the difference between the three regimes, demonstrating that at $\beta = 4.0$ the particles form the 18-fold quasicrystal. Further development of the 18-fold diffraction pattern at lower temperatures still and the temperature dependence of the bond-order correlations are given in the supporting material of reference [13]. Here the nature of the 18-fold order is additionally elaborated by examining the local packing motifs.

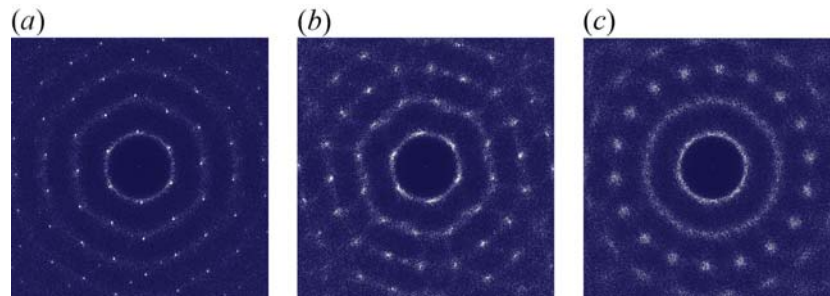


Figure 3. Fourier transforms of particles' centers of mass at $\beta = 3.0$ (a), 3.2 (b), and 4.0 (c) as representatives of the high-, intermediate-, and low-temperature regimes, respectively.

3. Frequencies of particle clusters

To this end, we classify the clusters of triangles and rhombi around a given vertex shown in figure 4. Each cluster is labeled by the corresponding vertex figure, a set of integers ($n_1.n_2.n_3.\dots$) that denotes the way that n_1 -gon, n_2 -gon, and n_3 -gon, \dots meet consecutively at each vertex [19]; and superscripts are employed to abbreviate the notation whenever possible.

We identify eight types of local clusters, which are more complex than those in the square-triangle dodecagonal tiling [20]. Three out of eight clusters (3^6 , $3^2.4.3.4$, and $3^3.4^2$) are the same as in the square-triangle tiling whereas the 4_a^4 and 4_b^4 clusters are both generalizations of the same 4^4 cluster of squares. In the former, rhombi are arranged either such that their long diagonals all point in the same direction and in the latter they form a chevron pattern. These five clusters may be constructed from rhombi of arbitrary shape and are thus referred to as the generic clusters. On the other hand, the special clusters only exist in 80° - 100° rhombi.

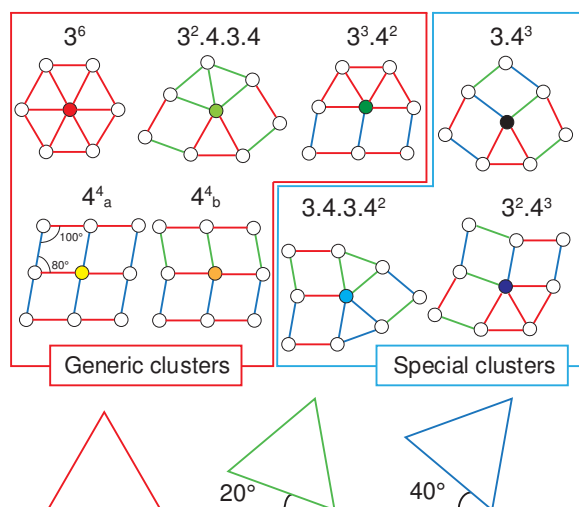


Figure 4. Classification of clusters in the 18-fold quasicrystal. The five generic clusters 3^6 , $3^2.4.3.4$, $3^3.4^2$, 4_a^4 , 4_b^4 appear in any rhombus-triangle tiling, whereas the three special clusters 3.4^3 , $3.4.3.4^2$, $3^2.4^3$ are characteristic of the 80° - 100° rhombus-triangle tiling. The red, green, and blue triangles at the bottom represent the three sets of bond orientations. The special clusters and the 4_b^4 cluster mix the three sets of orientations. The color code for vertices in the centers is used in figures 5, 7, and 8.

These clusters are needed so as to integrate the chevron cluster 4_b^4 into the matrix; the 3.4^3 accommodates its recessed side whereas the $3.4.3.4^2$ and $3^2.4^3$ accommodate its pointed side.

In figure 4, the edges appearing in the eight clusters are colored according to orientation. The 18-fold quasicrystal is marked by 18 bond directions which can be divided into three sets of 6 directions 60° apart and rotated with respect to each other by 20° . The three sets are conveniently represented by the red, green, and blue equilateral triangles drawn at the bottom of figure 4. The edge coloring shows that all generic clusters except 4_b^4 contain only orientations from two of these sets whereas the 4_b^4 cluster and all special clusters mix all three sets of bond orientations. This shows why they are key to understand the formation of 18-fold quasicrystals.

The frequencies of these eight cluster types is presented in figure 5, the special clusters all combined in a single class for clarity; also plotted is the frequency of all clusters beyond this classification. In a triangular tile, the overlap energy per particle of triangles is larger than in a rhombus. This explains why the frequency of the triangle-only 3^6 clusters decreases on cooling, whereas the frequencies of the 4_a^4 and 4_b^4 clusters is finite rather than 0 in the intermediate- and low-temperature regime at $\beta > 3.1$. On cooling towards $\beta = 3.1$, the frequencies of the 3^6 steadily decreases whereas those of the $3^2.4.3.4$ and the $3^3.4^2$ clusters increase. This is consistent with a decrease of the size of hexagonal domains. At the onset of the intermediate-temperature regime at $\beta = 3.1$, the frequencies of the $3^2.4.3.4$ and the $3^3.4^2$ clusters jump abruptly at the expense of the 3^6 clusters, which drops dramatically. We note that many local clusters do not belong to one of the 8 types in figure 4, and these are referred to as “other clusters” in figure 5.

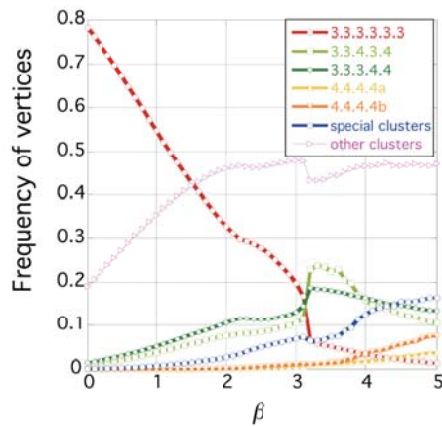


Figure 5. Frequencies of cluster types *vs.* β ; special and non-classified (“other”) clusters are plotted as single classes for clarity. At $\beta = 3.1$, abrupt changes of frequencies of several cluster classes are observed.

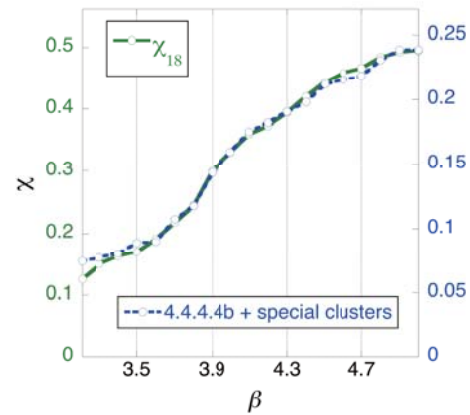


Figure 6. Superimposed 18-fold bond-orientational order parameter χ_{18} and the combined frequency of special and 4_b^4 clusters adapted from figures 2 and 5, respectively.

The gradual decrease of the frequencies of the $3^2.4.3.4$ and $3^3.4^2$ clusters and the concomitant increase of the frequency of special clusters on cooling beyond $\beta = 3.2$ are due to the different overlap energies of these clusters. All special clusters contain 3 rhombi whereas the $3^2.4.3.4$ and $3^3.4^2$ clusters contain only 2, and thus the former have a lower overlap energy than the latter. Also characteristic for the 2D 18-fold phase is a large frequency of clusters beyond the classification in figure 4, typically just a little short of 50 % as shown in figure 5.

These results all suggest that the onset of the 18-fold order parameter is closely correlated with the occurrence of the three special clusters, which are in turn needed for the integration

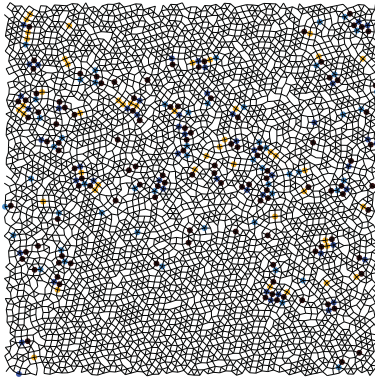


Figure 7. Coexistence of hexagonal and 18-fold phase at $\beta = 3.2$: The 4_b^4 and special clusters, which are color-coded like in figure 4, are not distributed uniformly.

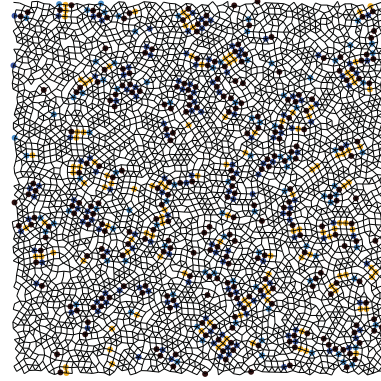


Figure 8. Spatial distribution of 4_b^4 and special clusters in the pure 18-fold phase at $\beta = 4.0$ is essentially uniform.

of the 4_b^4 clusters into the tiling. This correlation is best appreciated by plotting χ_{18} vs. β together with the combined frequencies of these four cluster types (figure 6), which shows that the two quantities are proportional to each other. The reason for this correlation is clear in representative snapshots of the system at $\beta = 3.2$ and $\beta = 4.0$ in figures 7 and 8, respectively. Here the clusters that mix the three sets of bond orientations are indicated by colored circles with yellow, sky blue, dark blue, and black corresponding to 4_b^4 , $3.4.3.4^2$, $3^2.4^3$, and 3.4^3 clusters, respectively. At $\beta = 3.2$ these clusters are present in the center band-region but not elsewhere, which is characteristic of phase coexistence expected in a constant-volume ensemble. At $\beta = 4.0$ they are distributed uniformly and this makes a complete 18-fold diffraction pattern. In both cases, many 4_b^4 clusters form short chains typically terminated by special clusters. We conclude that the frequency of the special clusters is proportional to the area occupied of the 18-fold region.

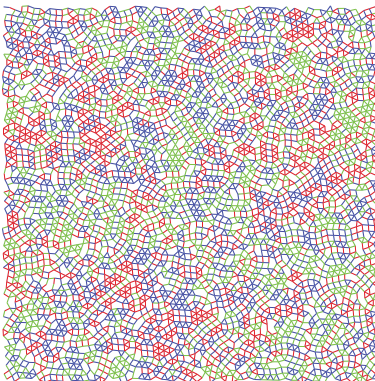


Figure 9. Snapshot from figure 8 redrawn by coloring the bonds according to the scheme defined at the bottom of figure 4. All three sets of directions are present.

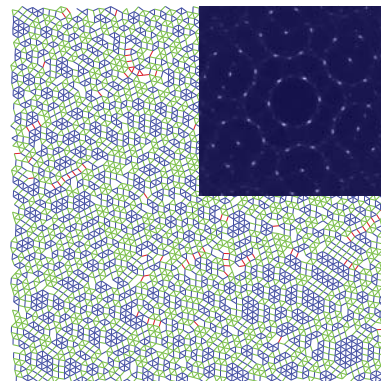


Figure 10. Colored-bond representation of the hexagonal phase at $\beta = 3.4$ and a packing fraction $\eta = 0.79$. Fourier transform emphasizes the 6-fold symmetry.

In figure 9, figure 8 is replotted by coloring the edges according to their orientation using the color scheme introduced by the three bond-direction triangles in figure 4. At $\beta = 4.0$, the three sets of directions are well mixed such that any small patch of the system has an 18-fold

symmetry. On close inspection, we see that the top and the bottom parts of figure 7 devoid of special clusters primarily consist of hexagonal domains separated by domain boundaries based on $3^3.4^2$ clusters. As a result, the hexagonal phase contains only two sets of bond orientations. This is more clearly seen in the system at a slightly larger packing fraction of $\eta = 0.79$ and a somewhat higher temperature of $\beta = 3.4$ where the stable state is purely hexagonal (figure 10).

4. Discussion

The above results elucidate the role of special clusters in the formation of the 18-fold quasicrystal, showing that they ensure that the three sets of bond orientations are equiprobable. Interestingly, two of our special clusters are also present in the dissection of a regular decaoctagon into 18 pentagons with internal angles of $60^\circ, 160^\circ, 80^\circ, 100^\circ$ and 140° provided that the pentagon is viewed as combination of an equilateral triangle and a $80^\circ - 100^\circ$ rhombus (figure 11a). This dissection can be admired in the intricate pattern on the facade of the Ravensbourne College in London, designed by Foreign Office Architects. The pattern appears to be derived from the 6-fold $18^2.3_{2\pi/9}^*$ decaoctagon-three-pointed star tiling [19] by shrinking the decaoctagons and dissecting them into the $60^\circ - 160^\circ - 80^\circ - 100^\circ - 140^\circ$ pentagons; the gaps between them are dissected into pentagons, triangles, and concave pentagons (figure 11b). The facade motif may be viewed as a hexagonal approximant of the 18-fold quasicrystal (plane group P6).

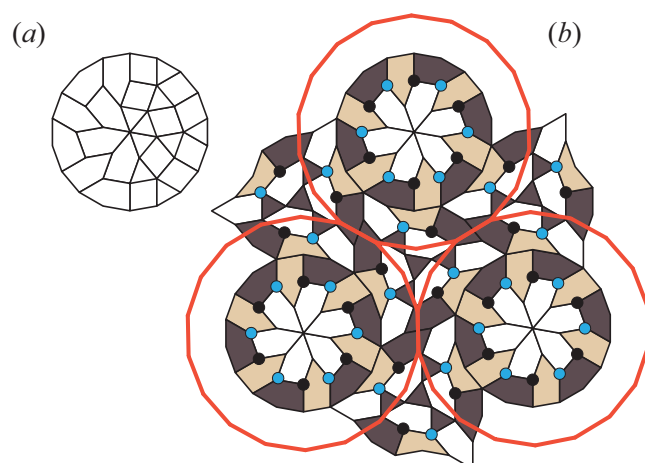


Figure 11. Dissection of the regular decaoctagon into irregular pentagons (a, left portion) which can be further divided into equilateral triangles and $80^\circ - 100^\circ$ rhombi (a, right portion). Motif from the Ravensbourne College (b). The red contours show a part of the underlying 6-fold $18^2.3_{2\pi/9}^*$ decaoctagon-three-pointed star tiling and its dissection. Also highlighted are the two special clusters $[3.4.3.4^2]$ (sky blue) and 3.4^3 (black) present in the motif.

Acknowledgments

This work was supported by Japan Society for the Promotion of Science [Grant-in-Aid for Scientific Research (B) No. 16H04037], by Slovenian Research Agency (Grant No. P1-0055), and by the Marie-Skłodowska-Curie European Training Network COLLDENSE (H2020-MSCA-ITN-2014 Grant No. 642774).

References

- [1] Zeng X, Ungar G, Liu Y, Percec V, Dulcey A E and Hobbs J K 2004 *Nature* **428** 157-160
- [2] Hayashida K, Dotera T, Takano A and Matsushita Y 2007 *Phys. Rev. Lett.* **98** 195502
- [3] Lee S, Bluemle M J and Bates F S 2010 *Science* **330** 351-353
- [4] Dotera T 2011 *Isr. J. Chem.* **51** 1197-1205
- [5] Fischer S, Exner A, Zielske K, Perlich J, Deloudi S, Steurer W, Lindner P and Förster S 2011 *Proc. Natl. Acad. Sci. USA* **108** 1810-1814

- [6] Janssen T, Chapuis G and de Boissieu M 2007 *Aperiodic crystals: From modulated phases to quasicrystals* (Oxford: Oxford University Press)
- [7] Steurer W & Deloudi S 2009 *Crystallography of quasicrystals: Concepts, methods and structures* (Berlin: Springer)
- [8] Young D A and Alder B J 1977 *Phys. Rev. Lett.* **38** 1213-1216
- [9] Jagla E A 1999 *J. Chem. Phys.* **110** 451-456
- [10] Malescio G and Pellicane G 2003 *Nat. Mater.* **2** 97-100
- [11] Glaser M A, Grason G M, Kamien R D, Košmrlj A, Santangelo C D and Zihlerl P 2007 *Europhys. Lett.* **78** 46004
- [12] Barkan K, Diamant H and Lifshitz R 2011 *Phys. Rev. B* **83** 172201
- [13] Dotera T, Oshiro T and Zihlerl P 2014 *Nature* **506** 208-211
- [14] Archer A J, Rucklidge A M and Knobloch E 2015 *Phys. Rev. E* **92** 012324
- [15] Pattabhiraman H, Gantapara A P and Dijkstra M 2015 *J. Chem. Phys.* **143** 164905
- [16] Ryltsev R, Klumov B and Chtchelkatchev N 2015 *Soft Matter* **11** 6991-6998
- [17] Schoberth H G, Emmerich H, Holzinger M, Dulle M, Förster S and Gruhn T 2016 *Soft Matter* **12** 7644-7654
- [18] Engel M and Glotzer S C 2014 *Nat. Phys.* **10** 185-186; Fig. 1 in this reference contains an artistic interpretation of the 18-fold quasicrystal by A. Šiber.
- [19] Grünbaum B and Shephard G C 2016 *Tilings and patterns*, 2nd Edition (New York: Dover)
- [20] Oxborrow M and Henley C L 1993 *Phys. Rev. B* **48**, 6966-6998